Density-Strength Decoupling in Compressed Earth Blocks: Insights from Mechanical, Ultrasonic, and Microstructural Characterisation

Amine Bouslihim
Laboratory of Mechanics and Materials, Faculty of Sciences, Mohammed V University, Rabat, Morocco | HESTIM Engineering & Business School, Center for Studies and Research in Engineering and Management (CERIM), Casablanca, Morocco
amine.bouslihim@um5r.ac.ma (corresponding author)

Hamid Bouabid
Laboratory of Mechanics and Materials, Faculty of Sciences, Mohammed V University, Rabat, Morocco
h.bouabid@um5r.ac.ma

Mohammed Cherraj
Team of Modelling and Simulating in Mechanics and Energetics, Faculty of Sciences, Mohammed V University, Rabat, Morocco
m.cherraj@um5r.ac.ma

Amine Bennis
HESTIM Engineering & Business School, Center for Studies and Research in Engineering and Management (CERIM), Casablanca, Morocco
abennis1@hestim.ma

Received: 14 February 2026 | Revised: 17 March 2026 | Accepted: 26 March 2026

 DOI: https://doi.org/10.48084/etasr.18168

ABSTRACT

This study investigates the effect of coarse sand grain correction on the coupled evolution of dry density, compressive strength, Ultrasonic Pulse Velocity (UPV), and microstructure of Compressed Earth Blocks (CEBs). Granular correction increased the Maximum Dry Density (MDD) from 1965 kg.m^{-3} to 2032 kg.m^{-3} (+3.4%); however, compressive strength decreased from 1.5 MPa to 1.25 MPa (-17%) and UPV from 0.873 km·s^{-1} to 0.737 km·s^{-1} (-16%). Conversely, a clay-rich soil exhibited the highest strength (2.42 MPa) and UPV (0.964 km·s^{-1}) despite the lowest density (1890 kg·m^{-3}). Scanning Electron Microscopy (SEM) and X-Ray Fluorescence (XRF) analyses revealed that strength evolution is governed primarily by the continuity of fines bonding rather than by density alone. A linear relationship between UPV and compressive strength was obtained with an R^2 = 0.803. These findings demonstrate a density-strength decoupling induced by physical particle size correction and highlight microstructural bonding as the controlling mechanism for low-carbon CEB optimization.

Keywords-compressed earth blocks; density-strength decoupling; particle-size distribution correction; ultrasonic pulse velocity; microstructural bonding; sustainable earthen materials

I. INTRODUCTION

Earthen materials range from traditional clay–straw mixtures to manufactured fired bricks. They are commonly produced in forms such as adobe, rammed earth, and CEBs. Interest in earthen construction has increased due to sustainability concerns associated with conventional fired masonry [1]. Fired clay brick production requires high energy input and generates significant carbon dioxide emissions, whereas unfired earth blocks consume less energy and produce fewer greenhouse gases [2, 3]. CEBs therefore represent a low-carbon alternative, benefiting from the use of locally available soils and reduced transportation impacts [4, 5]. However, their broader application remains limited due to the variability of natural soils and the difficulty of achieving adequate mechanical performance. In many cases, untreated soils fail to meet strength and durability requirements. While mechanical stabilization (compaction) and chemical stabilization (binders)

can improve performance, these methods increase both cost and embodied carbon [6]. Consequently, research has focused on physical optimization techniques to enhance block performance while maintaining low environmental impact [7-9]. Among these techniques, Particle Size Distribution (PSD) plays a critical role in determining CEB performance [10, 11]. The relative proportions of coarse and fine particles, as well as the continuity of the grading curve, directly influence packing density, porosity, and load transfer mechanisms within the material [12]. Previous studies indicate that a combined clay and silt content of approximately 25% is favorable for improving compressive strength, highlighting the importance of controlled PSD [13]. Furthermore, the addition of 5%–10% fine particles, combined with suitable stabilization, has been shown to produce blocks that meet industrial standards. These findings demonstrate that optimizing PSD is an effective strategy for enhancing block quality while promoting efficient resource utilization.

However, strong linear correlations between compressive strength and dry density, as well as between density and erosion resistance, have been reported [14]. Stabilization techniques can significantly modify dry density. For example, the incorporation of Calcium Carbide Residue (CCR) reduced bulk density from 1800 kg/m³ to 1475 kg/m³ while improving structural efficiency [15]. Despite the well-established influence of PSD and density on CEB performance, the underlying mechanisms linking density increase to strength development remain insufficiently understood. Although several studies report positive correlations between dry density and compressive strength [16], others demonstrate that changes in grading or stabilization can substantially alter density without a corresponding improvement in mechanical resistance. This suggests that density alone is not sufficient to explain the structural performance of CEBs [10, 17]. UPV is used as a non-destructive testing technique to assess the internal integrity and mechanical performance of geomaterials, owing to its correlation with stiffness, density, and compressive strength. UPV models can estimate compressive strength with high coefficients of determination, confirming the reliability of ultrasonic propagation as an indicator of mechanical behavior in cementitious and earth-based materials [18, 19]. Furthermore, UPV is sensitive to variations in soil composition and bonding structure, highlighting its relevance for evaluating earthen construction materials [20]. Despite these advances, the ability of UPV to capture density-strength decoupling induced in unstabilized CEBs remains insufficiently explored.

The present study examines the effect of coarse-grain correction, achieved by adding coarse sand, on the relationship between dry density, compressive strength, and UPV in CEBs made from natural soils. By integrating compaction analysis, mechanical testing, UPV measurements, and SEM/XRF microstructural characterization, it seeks to clarify the bonding mechanisms that control strength development after PSD modification. The main objective is to determine whether a density increase resulting solely from physical grain correction enhances mechanical performance, and to identify the microstructural constraints that limit density-based optimization strategies for low-carbon CEBs.

II. MATERIALS AND METHODS

The natural soils used in this study were collected from Sale (S), Marrakech (M), and Rabat (PR). The soils were air-dried and sieved before testing. PSD was determined using wet sieve analysis in accordance with [21], while the fine content was measured following [22]. Atterberg limits were determined according to [23] to characterize soil plasticity. The coarse sand used for granular correction was obtained from PR. The sand was washed and oven-dried before use to remove fine impurities. Table I presents the physical properties of the investigated materials. Soil S is mainly composed of sand (65%) with relatively low fines content (8% silt and 27% clay), resulting in low plasticity (PI = 11.5%). It also shows a lower Optimum water content (OWC) (8.5%) and a higher Maximum Dry Density (MDD) (1965 kg·m⁻³). In contrast, soil M contains a greater proportion of fines (30% silt and 33% clay), leading to higher plasticity (PI = 31.56%) and a higher OWC (12%), but a lower MDD (1890 kg·m⁻³). The sand PR consists entirely of coarse particles (100% sand) and exhibits no plasticity, making it appropriate for granular correction.

TABLE I. SOIL PHYSICAL PROPERTIES

Parameters		Soil S	Soil M	Sand PR
Grain size distribution	Sands	65%	37%	100%
	Silts	8%	30%	-
	Clays	27%	33%	-
Atterberg limits	Liquid limit (LL)	27.46%	47.24%	-
	Plastic limit (PL)	15.95%	15.68%	-
	Plasticity Index (PI)	11.5%	31.56%	-
Other parameters	OWC	8.5%	12%	-
	MDD	1965 kg·m^{-3}	1890 kg·m^{-3}	-

A. Sample Preparation

Initially, the soil mixtures were prepared by mixing the dry constituents corresponding to the three investigated materials: natural soil S, natural soil M, and the granular-corrected soil S+PR. For the corrected mixture (S+PR), the natural soil S was combined with 32% coarse sand PR by dry mass (68% S), following a previously developed granular optimization protocol based on CRATerre admissible grading envelopes and an iterative geometric-mean target curve ensuring a maximum particle size of 5 mm [24]. This granular correction increased the MDD from 1965 kg·m⁻³ for the initial soil to 2032 kg·m⁻³ for the corrected mixture. All dry components were mixed thoroughly to ensure homogeneous distribution. Water was then gradually added to each mixture until the OWC was reached. The OWC was determined by compacting each soil type at different water contents and measuring the corresponding dry density until the MDD was obtained.

Samples were prepared using cylindrical molds with dimensions of 8 cm in diameter and 12 cm in height. For each soil type or mixture, five specimens were compacted using a manual hydraulic press at a pressure of 2 MPa. After molding, the samples were sealed in plastic bags and cured for 7 days, followed by storage under laboratory conditions for an additional 21 days. During this period, the ambient temperature

ranged from 19°C to 25°C, and the relative humidity varied between 55% and 70%. Figure 1 shows the PSD of soils S, M, and PR compared with the CRATerre proposed grading envelope. Soil S lies near the lower limit of fines content, while soil M is finer and closer to the upper boundary. In contrast, sand PR consists almost entirely of coarse particles and falls outside the proposed range. The corrected mixture (S+PR) shifts the grading toward coarser fractions, increasing packing density but reducing fines responsible for interparticle bonding. The dashed lines indicate the limits of the proposed grading range [25].

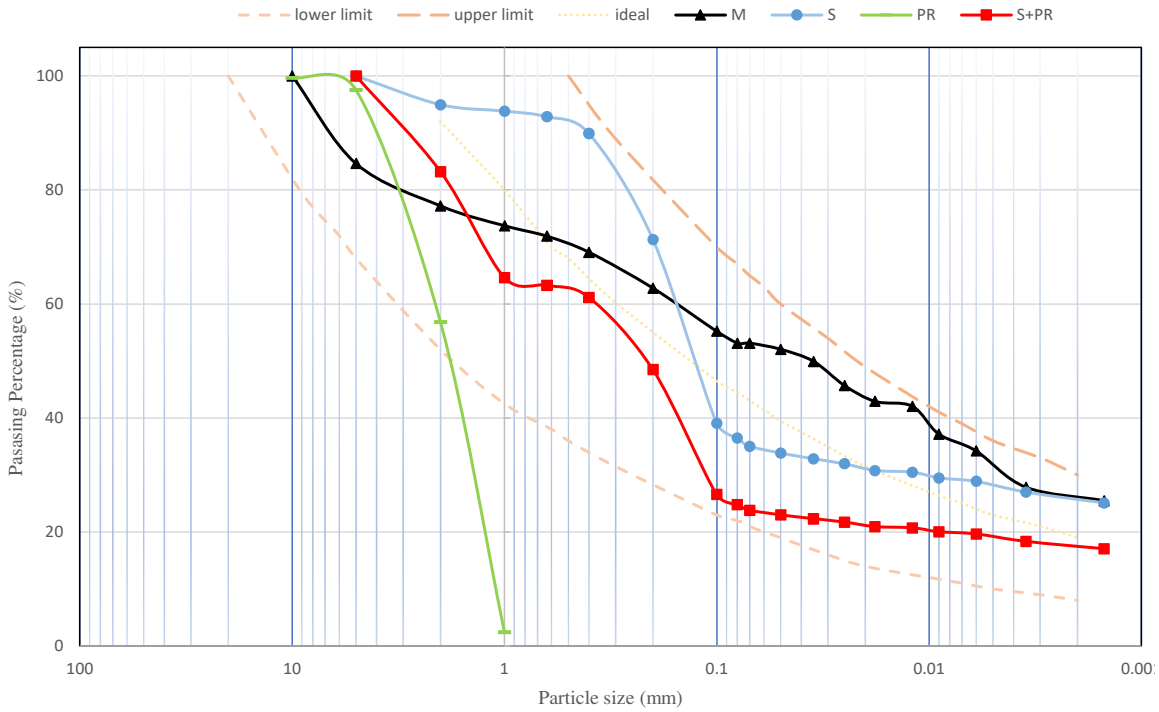

Fig. 1. PSD of soils S, M, and PR compared with CRATerre recommendations for CEB production.

B. Testing Methods

Figure 2 illustrates the four types of experimental equipment used in this study to characterize the physical, mechanical, and microstructural properties of the samples. These include XRF for chemical composition analysis, SEM for microstructural observation, UPV testing for non-destructive evaluation of internal integrity, and a universal testing machine for compressive strength measurement.

- Compressive strength tests were performed according to standard procedures using a Tinius Olsen ST universal testing machine. The specimens were subjected to uniaxial compressive loading until failure, and the load measurements were recorded. The compressive strength was calculated by dividing the maximum load by the cross-sectional area of each specimen. Visual examinations were also conducted to identify the failure pattern and to observe any differences in rupture modes among the soil samples.
- Small representative fragments were prepared for observation using a JSM-IT510 SEM and used to characterize the material at a microscale for global texture analysis, particle packing, pore distribution, the arrangement of coarse and fine fractions, and fine bonding zones.

Fig. 2. Experimental testing equipment used in the study: (a) XRF analysis, (b) SEM observation, (c) UPV measurement, and (d) compressive strength test.

- XRF analysis was performed, using a Bruker S2 Ranger spectrometer, to determine the chemical composition of the soil samples, identify the major oxide components, and provide information on the mineralogical composition influencing the mechanical behavior of the CEBs.
- UPV measurements were carried out using a U300 ultrasonic tester equipped with 50 kHz transducers. The direct transmission method was adopted. The transducers were placed on opposite faces of the specimens, and coupling gel was applied to ensure proper signal transmission. For each specimen, three travel time measurements were recorded to improve accuracy. Measurements were performed at room temperature under dry surface conditions, and the UPV was calculated by dividing the specimen length by the measured travel time.

III. RESULTS AND DISCUSSION

A. *Effect of Granular Correction on MDD and Compressive Strength*

As Table II summarizes, the natural soil S exhibited an MDD of 1965 kg·m⁻³ and a compressive strength of 1.5 MPa, with a particle composition dominated by sand (65%) and a moderate clay content (27%). Following granular correction by the addition of coarse sand (S+PR), the sand fraction increased to 76% while the clay content decreased to 18%. This modification led to a 3.4% increase in MDD (2032 kg·m⁻³); however, the compressive strength decreased by 17% to 1.25 MPa. This inverse trend between density and strength indicates that the improved packing efficiency was accompanied by a reduction in effective interparticle bonding, due to the lower proportion of fine particles. Such behavior is consistent with [10], which demonstrates that particle-size distribution and clay content can have a greater influence on strength and stiffness than dry density alone.

TABLE II. SUMMARY OF PHYSICAL AND MECHANICAL PROPERTIES OF THE INVESTIGATED SOILS (MEAN ± STANDARD DEVIATION, N (NUMBER OF SAMPLES) = 5)

Soil	MDD (kg·m^{-3})	Compressive strength (MPa)	UPV (km·s^{-1})
S	1965	1.50 ± 0.072	0.873 ± 0.012
S+PR	2032	1.25 ± 0.12	0.737 ± 0.011
M	1890	2.42 ± 0.099	0.964 ± 0.012

Soil M, with high fines content (30% silt and 33% clay), exhibited the highest compressive strength of 2.42 MPa, despite having the lowest MDD (1890 kg·m^{-3}). Relative to soil S, this corresponds to a 4% decrease in density but a 61% increase in strength, while the strength gain reached 94% compared with S+PR.

B. *Microstructural Analysis (SEM and XRF)*

The SEM observations of soil S (Figure 4(a)) reveal localized clay platelet coatings partially covering coarse particles (P2), together with discontinuous interparticle bridges (P3) and inter-aggregate microporosity (P1), consistent with previous microstructural studies highlighting the role of clay platelet bonding and pore distribution in governing cohesion and strength in unfired clay bricks [26]. The S+PR microstructure (Figure 4(b)) remains dominated by coarse granular clusters (P4) separated by intergranular voids lacking clay bonding (P5). This configuration supports the 3%–4% increase in dry density obtained after correction, which is associated with reduced fines-controlled cohesion and provides direct microstructural evidence for the 17% decrease in compressive strength. Soil M (Figure 4(c)) exhibits a continuous clay platelet network (P6) reinforced by fibrillar or filamentous inter-platelet bridges (P7), producing an interconnected bonding framework. Such structural continuity promotes efficient stress transfer throughout the compacted matrix, corresponding to the 61% higher compressive strength of soil M relative to soil S, despite its lower MDD, consistent with the mechanisms reported in [27, 28].

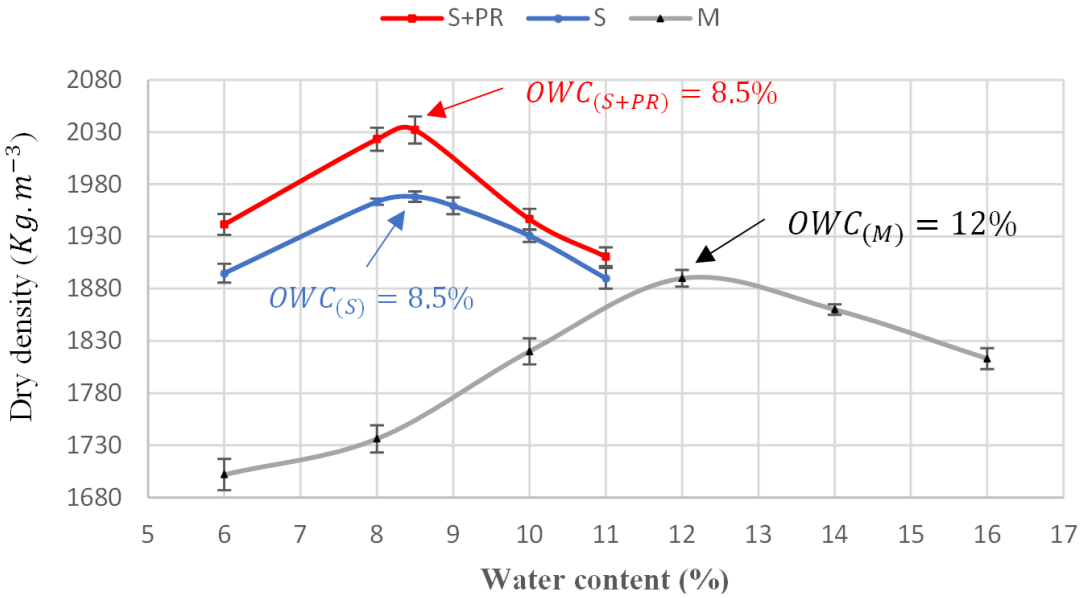

Fig. 3. Compaction curves of soils S, S+PR, and M, showing OWC content at MDD.

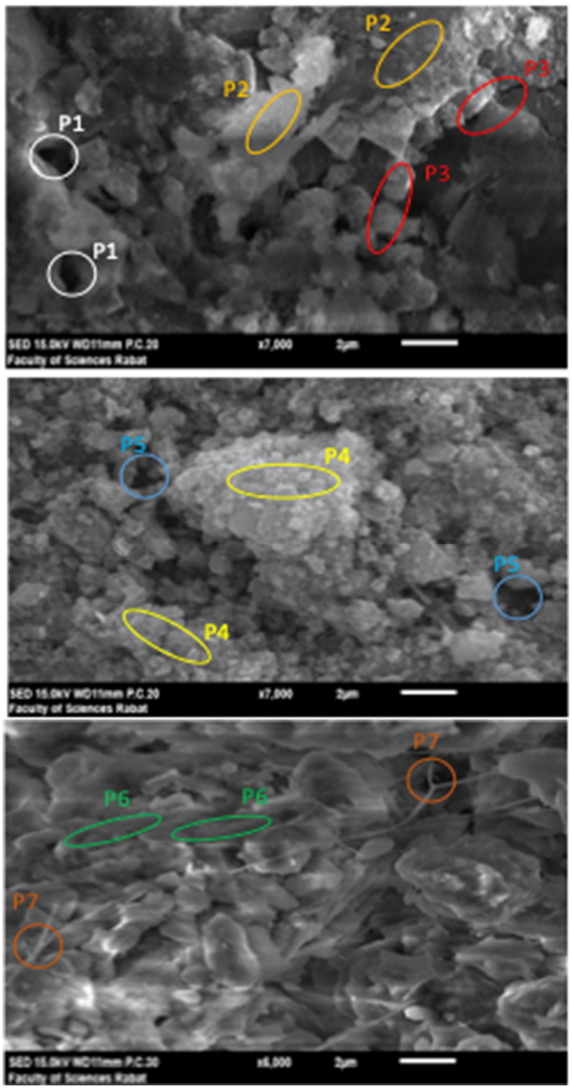

Fig. 4. SEM microstructures of soils: (a) soil S showing microporosity (P1), partial clay platelet coatings (P2), and discontinuous interparticle bridges (P3); (b) granular corrected soil S+PR characterized by coarse particle clusters (P4) and intergranular voids lacking clay bonding (P5); (c) soil M exhibiting a continuous clay platelet network (P6) and fibrillar bonding features (P7).

TABLE III. OXIDE COMPOSITION DETERMINED BY XRF

Oxide	M (%)	S (%)
Na_2O	1.8	0
MgO	7	1.2
Al_2O_3	15.91	23.81
SiO_2	48.83	51.57
P_2O_5	0.09	0.09
SO_3	0.18	0.26
Cl	0.06	0
K_2O	3.85	1.72
CaO	11.36	1.32
TiO_2	1.3	1.36
MnO	0.14	0
Fe_2O_3	8.96	18.01
ZrO_2	0.09	0.14
BaO	0.14	0
Pr_6O_{11}	0	0.06
Nd_2O_3	0	0.08

The XRF analysis, summarized in Table III, further supports the microstructural observations. Soil M exhibits significantly higher CaO (11.36%) and MgO (7%) contents compared to soil S (1.32% and 1.2%, respectively), corresponding to increases of approximately 8–9 times for CaO and about sixfold for MgO, while maintaining similar SiO_2 contents. In clayey soils, elevated concentrations of divalent cations, such as Ca^{2+} and Mg^{2+}, promote the flocculation of clay particles and the formation of microaggregates. This occurs through the displacement of monovalent ions from exchange sites and the compression of the diffuse double layer, resulting in stronger electrostatic attraction and reduced particle dispersion [29]. Consequently, soil S, which contains lower amounts of these divalent cations, exhibits weaker clay aggregation than soil M, as confirmed by the SEM observations. This difference in microstructural bonding is consistent with the 61% higher compressive strength measured for soil M.

C. UPV as an Indicator of Bonding Continuity

The natural soil S exhibited an average UPV of 0.873 km·s^{-1}, whereas the granular-corrected mixture S+PR showed a lower value of 0.737 km·s^{-1}, representing a decrease of approximately 16% despite the increase in MDD. In contrast, soil M displayed the highest UPV (0.964 km·s^{-1}), corresponding to an increase of about 10% relative to soil S, and more than 30% compared to S+PR, even though it had the lowest dry density among the tested soils. As illustrated in Figures 5 and 6, the trends in compressive strength and UPV are consistent, highlighting the strong link between ultrasonic propagation and mechanical performance. This behavior reflects the presence of a dense, clay-rich bonding network observed in SEM analysis and supported by the XRF results, enhancing wave transmission through continuous interparticle contact paths.

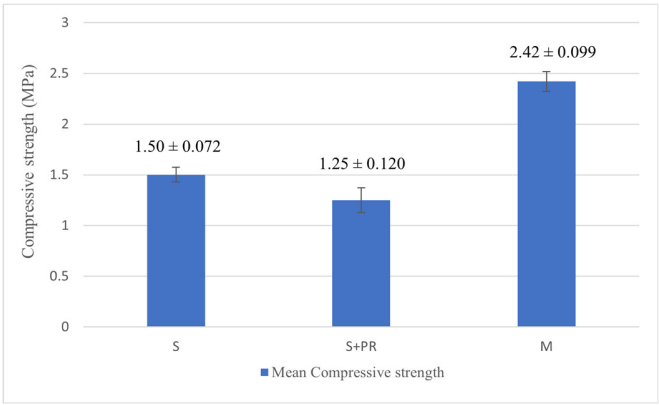

Fig. 5. Mean compressive strength of the investigated soils. Error bars represent standard deviation (n = 5).

D. Relationship Between UPV and Compressive Strength

A linear relationship was obtained between UPV and compressive strength for CEB specimens, expressed as:

$$f_c = 4.88\,\mathrm{UPV} - 2.46 \quad (1)$$

With a coefficient of determination:

$$R^2 = 0.803 \ (n = 15) \quad (2)$$

where n denotes the number of tested specimens.

This value indicates that approximately 80% of the variability in compressive strength can be explained by variations in ultrasonic wave propagation. The obtained R^2 of 0.803 lies within the upper range typically reported for earthen construction materials, which generally fall between 0.6 and 0.9, depending on density, stabilization level, and water content. The regression slope of 4.88 MPa·s·km^{-1} reflects the mechanical sensitivity of strength to the change in ultrasonic velocity. This magnitude is consistent with previously reported linear sensitivities in rammed earth and CEBs, which commonly range from approximately 3 MPa·s·km^{-1} to 6 MPa·s·km^{-1} for unstabilized or weakly stabilized blocks.

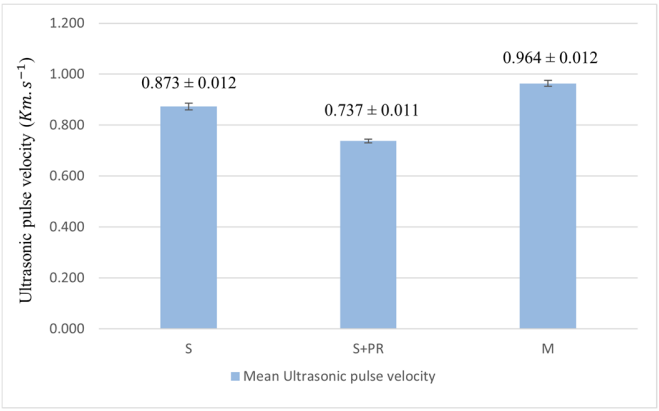

Fig. 6. Mean UPV of the investigated soils. Error bars represent standard deviation (n = 5).

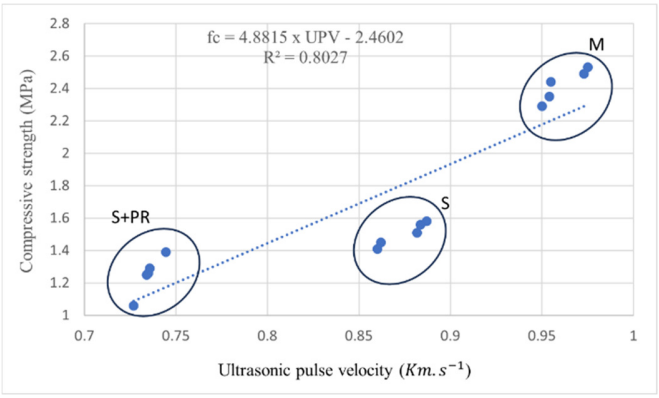

Fig. 7. Relationship between UPV and compressive strength of CEBs.

As presented in Figure 7, the investigated UPV range (0.73–0.98 km·s^{-1}) corresponds to a transition from weakly bonded granular structures to more continuous clay-bonded matrices. This evolution is accompanied by an increase in compressive strength from approximately 1.1 MPa to 2.5 MPa. The observed relationship indicates that ultrasonic wave propagation reflects the quality of interparticle contacts and the reduction of internal discontinuities, rather than density alone. Overall, the comparison between soils S, S+PR, and M confirms that mechanical performance is not governed solely by density but is more significantly influenced by the combined effect of particle-size distribution and the continuity of fines-mediated bonding.

IV. CONCLUSIONS

This study investigated the effect of coarse-grain physical correction on the coupled evolution of dry density, compressive strength, UPV, and microstructure of Compressed Earth Blocks (CEBs) made from natural soils. Granular correction increased the MDD from 1965 to 2032 kg·m^{-3} (+3.4%), but resulted in a decrease in compressive strength from 1.5 to 1.25 MPa (−17%) and in UPV from 0.873 to 0.737 km·s^{-1} (−16%). In contrast, the clay-rich soil from Marrakech exhibited the highest compressive strength (2.42 MPa) and UPV (0.964 km·s^{-1}), despite having the lowest density (1890 kg·m^{-3}). These results show that mechanical performance cannot be explained by densification alone. Microstructural analysis indicates that strength is mainly controlled by the continuity of fines-mediated bonding and interparticle cohesion. SEM and XRF observations confirm that granular correction disrupts clay bonding networks, whereas the clay-rich soil develops a continuous platelet structure that improves stress transfer and facilitates ultrasonic wave propagation. A strong linear relationship between UPV and compressive strength (R^2 = 0.803) further indicates that ultrasonic measurements effectively capture microstructural integrity and can be used to predict mechanical performance. Overall, the findings reveal a clear density–strength decoupling induced by particle-size distribution correction, highlighting the crucial role of bonding continuity in controlling CEB behavior. This study underscores the limitations of density-based optimization, emphasizing the need to consider both particle-size distribution and fines-mediated bonding in the design of low-carbon earthen materials.

Beyond the specific experimental results, the current study contributes to understanding the mechanical behavior of CEBs by emphasizing a density-strength decoupling associated with particle-size distribution correction. While previous studies generally report positive correlations between density and strength in earthen materials, the present work's results indicate that an increase in packing density, achieved through coarse-grain addition, may not necessarily result in improved mechanical performance when the fines content is reduced. The combined analysis of mechanical testing, UPV measurements, and microstructural observations suggests that variations in strength are closely related to changes in the continuity of fines-mediated bonding within the material. In this context, ultrasonic wave propagation appears to reflect the integrity of interparticle contacts and internal structure beyond density variations alone. These findings provide additional insights into the limitations of density-based optimization approaches, stressing the importance of considering both particle-size distribution and bonding continuity in the design and characterization of low-carbon CEBs.

DECLARATION OF COMPETING INTERESTS

The authors declare that they have no potential conflicts of interest with respect to the research, authorship, and/or publication of this article.

ACKNOWLEDGMENT

The authors received partial financial support from CERIM to cover the publication fees.

DATA AVAILABILITY

All data generated or analyzed during this study are included in this published article.

REFERENCES

[1] D. Gandreau and L. Delboy, *World heritage inventory of earthen architecture*. France: CRATerre-ENSAG, 2012.

[2] A. C. Paula Junior, E. Teixeira, and R. Mateus, "Improving the mechanical, thermal and durability properties of compressed earth blocks by incorporating industrial waste and by-products: A systematic literature review," *Construction and Building Materials*, vol. 438, Aug. 2024, Art. no. 137063, https://doi.org/10.1016/j.conbuildmat.2024.137063.

[3] M. Dabaieh, J. Heinonen, D. El-Mahdy, and D. M. Hassan, "A comparative study of life cycle carbon emissions and embodied energy between sun-dried bricks and fired clay bricks," *Journal of Cleaner Production*, vol. 275, Dec. 2020, Art. no. 122998, https://doi.org/10.1016/j.jclepro.2020.122998.

[4] M. Valenzuela *et al.*, "Towards the development of performance-efficient compressed earth blocks from industrial and agro-industrial by-products," *Renewable and Sustainable Energy Reviews*, vol. 194, Apr. 2024, Art. no. 114323, https://doi.org/10.1016/j.rser.2024.114323.

[5] R. Mateus, J. Fernandes, and E. R. Teixeira, "Environmental life cycle analysis of earthen building materials," *Encyclopedia of Renewable and Sustainable Materials*, vol. 4, pp. 63–68, 2020.

[6] A. T. Shiferaw, "Carbon Conscious Construction: Evaluating Compressed Stabilized Earth Blocks," *Buildings*, vol. 15, no. 23, Dec. 2025, https://doi.org/10.3390/buildings15234362.

[7] S. N. Malkanthi, A. A. D. A. J. Perera, G. H. Galabada, and P. D. Dharmaratne, "Enhancement of the Properties of Compressed Stabilized Earth Blocks through the Replacement of Clay and Silt with Fly Ash," *Engineering, Technology & Applied Science Research*, vol. 11, no. 6, pp. 7927–7931, Dec. 2021, https://doi.org/10.48084/etasr.4580.

[8] S. N. Malkanthi and A. A. D. A. J. Perera, "Particle Packing Application for Improvement in the Properties of Compressed Stabilized Earth Blocks with Reduced Clay and Silt," *Engineering, Technology & Applied Science Research*, vol. 9, no. 4, pp. 4538–4542, Aug. 2019, https://doi.org/10.48084/etasr.3002.

[9] A. Bennis *et al.*, "Improving Mechanical Properties of Compressed Earth Blocks Through Wet Granular Correction," *JP Journal of Heat and Mass Transfer*, vol. 37, no. 6, pp. 843–860, Nov. 2024, https://doi.org/10.17654/0973576324052.

[10] A. Cuccurullo, D. Gallipoli, A. W. Bruno, C. Augarde, P. Hughes, and C. La Borderie, "A comparative study of the effects of particle grading and compaction effort on the strength and stiffness of earth building materials at different humidity levels," *Construction and Building Materials*, vol. 306, Nov. 2021, Art. no. 124770, https://doi.org/10.1016/j.conbuildmat.2021.124770.

[11] G. Ruiz, X. Zhang, W. F. Edris, I. Cañas, and L. Garijo, "A comprehensive study of mechanical properties of compressed earth blocks," *Construction and Building Materials*, vol. 176, pp. 566–572, July 2018, https://doi.org/10.1016/j.conbuildmat.2018.05.077.

[12] E. R. Teixeira *et al.*, "Mechanical and Thermal Performance Characterisation of Compressed Earth Blocks," *Energies*, vol. 13, no. 11, June 2020, https://doi.org/10.3390/en13112978.

[13] S. N. Malkanthi, W. G. S. Wickramasinghe, and A. A. D. A. J. Perera, "Use of construction waste to modify soil grading for compressed stabilized earth blocks (CSEB) production," *Case Studies in Construction Materials*, vol. 15, Dec. 2021, Art. no. e00717, https://doi.org/10.1016/j.cscm.2021.e00717.

[14] H. Danso, "Influence of Compacting Rate on the Properties of Compressed Earth Blocks," *Advances in Materials Science and Engineering*, vol. 2016, no. 1, Jan. 2016, Art. no. 8780368, https://doi.org/10.1155/2016/8780368.

[15] P. Nshimiyimana, N. Fagel, A. Messan, D. O. Wetshondo, and L. Courard, "Physico-chemical and mineralogical characterization of clay materials suitable for production of stabilized compressed earth blocks," *Construction and Building Materials*, vol. 241, Apr. 2020, Art. no. 118097, https://doi.org/10.1016/j.conbuildmat.2020.118097.

[16] A. W. Bruno, D. Gallipoli, C. Perlot, and J. Mendes, "Mechanical behaviour of hypercompacted earth for building construction," *Materials and Structures*, vol. 50, no. 2, Mar. 2017, Art. no. 160, https://doi.org/10.1617/s11527-017-1027-5.

[17] C. Turco, A. P. Junior, C. Jacinto, J. Fernandes, E. Teixeira, and R. Mateus, "Influence of Particle Size on Compressed Earth Blocks Properties and Strategies for Enhanced Performance," *Applied Sciences*, vol. 14, no. 5, Feb. 2024, https://doi.org/10.3390/app14051779.

[18] A. Nazari and V. Toufigh, "Prediction of ultrasonic pulse velocity and physicochemical properties of rice husk ash concrete exposed to elevated temperatures and post-fire curing," *Case Studies in Construction Materials*, vol. 24, July 2026, Art. no. e05715, https://doi.org/10.1016/j.cscm.2025.e05715.

[19] F. J. Ávila Cruces, M. E. Puertas García, and R. Gallego Sevilla, "Mechanical characterization of lime-stabilized rammed earth: Lime content and strength development," July 2022, https://doi.org/10.1016/j.conbuildmat.2022.128871.

[20] S. S. D. Raavi and D. D. Tripura, "Ultrasonic pulse velocity and statistical analysis for predicting and evaluating the properties of rammed earth with natural and brick aggregates," *Construction and Building Materials*, vol. 298, Sept. 2021, Art. no. 123840, https://doi.org/10.1016/j.conbuildmat.2021.123840.

[21] NF P 94-056 Analyse granulométrique par tamisage. France: AFNOR, 1996.

[22] NF P 94-057 Granulométrie - Méthode Par Sédimentation. France: AFNOR, 1992.

[23] NF P94-051 Détermination des limites d'Atterberg. France: AFNOR, 1993.

[24] A. Bouslihim *et al.*, "Optimizing Soil Particle Distribution for Improved Compressed Earth Block Performance: A Mixing Approach," *JP Journal of Heat and Mass Transfer*, vol. 37, no. 6, pp. 791–806, Nov. 2024, https://doi.org/10.17654/0973576324049.

[25] *Compressed Earth Blocks: Standards*. Centre for the Development of Industry, 1998.

[26] J. E. Oti, J. M. Kinuthia, and J. Bai, "Compressive strength and microstructural analysis of unfired clay masonry bricks," *Engineering Geology*, vol. 109, no. 3, pp. 230–240, Nov. 2009, https://doi.org/10.1016/j.enggeo.2009.08.010.

[27] P. J. Walker, "Strength and Erosion Characteristics of Earth Blocks and Earth Block Masonry," *Journal of Materials in Civil Engineering*, vol. 16, no. 5, pp. 497–506, Oct. 2004, https://doi.org/10.1061/(ASCE)0899-1561(2004)16:5(497).

[28] H. Houben and H. Guillaud, *Traité de construction en terre*. Parenthèses, 1989.

[29] W.-Y. Sun, H. Zeng, and T. Tang, "Mechanisms for clay-polymer interactions in the treatment of mature fine tailings: A review," *Petroleum Science*, vol. 21, no. 6, pp. 4427–4445, Dec. 2024, https://doi.org/10.1016/j.petsci.2024.10.002.